Sensors and Actuators B 220 (2015) 68–74

Contents lists available at ScienceDirect

Sensors and Actuators B: Chemical

journal homepage: www.elsevier.com/locate/snb

Vitamin C-assisted synthesis and gas sensing properties of coaxial In_2O_3 nanorod bundles

Xiaowei Li, Shiting Yao, Jiangyang Liu, Peng Sun*, Yanfeng Sun, Yuan Gao, Geyu Lu*

State Key Laboratory on Integrated Optoelectronics, College of Electronic Science and Engineering, Jilin University, 2699 Qianjin Street, Changchun 130012, China

ARTICLE INFO

Article history:
Received 9 March 2015
Received in revised form 7 May 2015
Accepted 17 May 2015
Available online 28 May 2015

Keywords:
Gas sensor
NO_2
Microwave hydrothermal
In_2O_3
Nanorod bundles

ABSTRACT

In_2O_3 nanorod bundles with well-designed morphology, hierarchical nanostructure and large specific surface area were quickly prepared via microwave hydrothermal method in the presence of vitamin C. The observations of field emission electron microscopy and transmission electron microscopy revealed that the as-prepared In_2O_3 samples were constructed from lots of well-aligned nanorods with average diameter of about 50 nm. To demonstrate their potential application in detecting harmful gases, these bundle-like In_2O_3 samples were applied to fabricate gas sensor and their sensing properties were examined. It was found that the sensors based on such novel In_2O_3 nanorod bundles exhibited high response and excellent selectivity during detecting NO_2 gas at the operating temperature of 100 °C.

1. Introduction

Over the past decades, the design and development of gas sensors with high sensing performance has been a research hotspot due to its profound influence on human health and environmental protection [1]. Thanks to the advances in nanotechnologies and synthetic methods, various kind of sensing materials, such as metal-oxide semiconductors, polymers, carbon nanotubes, and moisture absorbing materials, have been developed and applied in gas sensors [2–5]. Among them, the sensors based on metal-oxide semiconductors have triggered great interest owing to their attractive characteristics such as low cost, high sensitivity, and controllable preparation [6–8]. Indium oxide (In_2O_3), an important n-type oxide semiconductor with wide direct band gap of 3.55–3.75 eV at room temperature [9], has been recognized as an ideal functional material and widely used in detecting hazardous gases like NH_3, CO, H_2S, NO_x and so on [10–18]. It is well known that the properties of metal-oxide semiconductors can be optimized by tailoring their morphology, aspect ratio, size, crystal orientation, and density of defects [19–21]. In this context, rational synthesis of novel nanostructures is thus of vital importance to improve the sensing performance of In_2O_3 nanocrystals.

As a new class of special three-dimensional (3D) structures, hierarchical nanostructures that are constructed from many low dimensional building blocks have attracted a great deal of research interest because of their well-defined configurations and intriguing properties. It has been demonstrated that an increase in utility factor of the sensing material can considerably improve the sensing performance of gas sensor [22]. The periodically assembled building blocks endow hierarchical nanostructures with abundant porous structures and high surface area, which can allow the gas molecules diffuse rapidly and effectively through the sensing materials [23]. Therefore, the hierarchical nanostructures are hopeful to become a new generation of ultra sensitive gas sensing materials. Recently, as motivated by the driving force of developing gas sensors with high sensitivity, good selectivity and low detection limit, numerous methods such as template-directed [24], thermal evaporation [25,26], chemical vapour deposition (CVD) [27] and solution-based approaches [28–30], have been employed to prepare hierarchical nanostructures with diverse building blocks. However, in most cases, the above-mentioned synthetic methods may suffer from many serious drawbacks including tedious synthesis procedures, sophisticated equipments, toxic chemical reagents and rigid experimental conditions. Therefore, an efficient, facile and green method is still required in view of all above considerations. Microwave-assisted synthesis, as a promising strategy, has gained tremendous attention because it not only provides homogeneous and efficient heating source to help increasing the temperature of the entire reaction vessel simultaneously and rapidly, but also can

* Corresponding author. Tel.: +86 431 85167808; fax: +86 431 85167808.
E-mail addresses: spmaster2008@163.com (P. Sun), lugy@jlu.edu.cn (G. Lu).

http://dx.doi.org/10.1016/j.snb.2015.05.038
0925-4005/

make the synthesis reaction under precise control by virtue of its small thermal inertia [31,32]. Thus, these effects make microwave-assisted synthesis particularly suitable to prepare high-quality delicate nano-materials.

In this contribution, a microwave hydrothermal method using vitamin C as structure-directing agent was reported for the rapid synthesis of In_2O_3 nanorod bundles. The synthesis procedure was performed in aqueous solvent with a short reaction time (30 min). The formation mechanism of In_2O_3 nanorod bundles was proposed on the basis of the time-dependent morphologies of In_2O_3 samples. In addition, the nitrogen dioxide (NO_2) sensing performances of sensors based on resulting In_2O_3 were systematically examined.

2. Experimental

All the reagents in current experiment were analytical grade and directly used as purchased without any further purification. In a typical procedure, a transparent aqueous solution (30 mL) containing 1 mmol of indium chloride tetrahydrate ($InCl_3{\cdot}4H_2O$) and 5 mmol of urea ($CO(NH_2)_2$) was first prepared at room temperature. Then, 0.125 mmol of ascorbic acid ($C_6H_8O_6$, vitamin C) was added into the above solution as a structure-directing agent. After vigorous stirring for 15 min, the resulting mixture was transferred into a 100 mL Teflon-lined autoclave and treated with a predetermined heating procedure (first heated to 140 °C at a heating rate of 4 °C min^{-1} from room temperature, then cooled down naturally) in a microwave hydrothermal system. After that, the precipitates were harvested with the assistance of centrifugation and washed with deionized water and absolute ethanol for several times, then dried in air at 80 °C for 5 h. To obtain the pure In_2O_3 samples, the precipitates were finally calcined at 550 °C for 2 h in muffle furnace.

X-ray diffraction (XRD) patterns were recorded by Rigaku D/max-2550 diffractometer (operated at 40 kV per 200 mA) with Cu Kα radiation (λ = 1.5406 Å) in the range of 20–80° (2θ). Field emission scanning electron microscopy (FESEM) images were taken on a JEOL JSM-7500F microscope, which was operated at 15 kV. Transmission electron microscopy (TEM) and high resolution transmission electron microscopy (HRTEM) observations were performed on a JEOL JEM-2100F microscopy with an accelerating voltage of 200 kV. Nitrogen adsorption–desorption isotherm was measured on a Gemini VII surface area and porosity system at 77 K. The specific surface area was estimated using the Brunauer-Emmett-Teller (BET) equation based on the nitrogen adsorption isotherm. Pore diameter distribution was calculated by Barrett–Joyner–Halenda (BJH) method using the adsorption branch of the isotherms.

The detailed fabrication and measurement of gas sensor were similar to the methods reported in our previous works [33,34]. Briefly, a ceramic tube (4 mm in length, 1.2 mm in external diameter, and 0.8 mm in internal diameter) with a pair of gold electrodes and four platinum wires was first prepared as substrate. The as-synthesized In_2O_3 powder was uniformly dispersed in the deionized water to form a paste, and then coated on the above ceramic tube. After drying in air at room temperature, the device was transferred into muffle furnace and aged at 400 °C for 2 h to improve the thermal stability of the sensor. Subsequently, a Ni-Cr heating coil was inserted through the ceramic tube to control the operating temperature of sensor.

The electrical properties of the sensor were measured by a static process: the sensor was placed in a test chamber full of fresh air at the beginning, and then a given amount of test gas was injected into the chamber by an injector. After the response reaching a steady value, the sensor was transferred into another chamber also full of air and began to recover. According to the chemical properties of different test gases, the response (S) of sensor was defined as $S = R_g/R_a$ (for oxidizing test gases) and $S = R_a/R_g$ (for reducing test gases), respectively. Here, R_a and R_g were the resistances of the sensor when exposed in the air and test gas atmosphere. The time taken by the sensor to achieve 90% of the total resistance change in the case of adsorption and desorption were designated as the response time and recovery time, respectively.

3. Results and discussion

3.1. Morphology and composition analysis

Fig. 1 shows the X-ray diffraction (XRD) pattern of the as-prepared In_2O_3 powder. As can be seen, all of the diffraction peaks were matched well with those from the standard JCPDS card no. 6-416 (space group: Ia-3), indicating that the obtained powder could be indexed as cubic In_2O_3 with lattice parameters of a = 10.118 Å. Besides, no other crystalline phase corresponding to impurity was detected, indicating that the product had a high purity. Furthermore, the average crystallite size of obtained In_2O_3 was calculated to be about 18 nm using the Debye–Scherrer formula: $D = 0.89\lambda/(\beta\cos\theta)$, where λ represents the X-ray wavelength (1.5406 Å for Cu Kα radiation), θ is the Bragg diffraction angle, and β represents the peak width at half maximum.

The microstructures and morphologies of the as-synthesized In_2O_3 sample were investigated by FESEM observations. As can be seen from the panoramic FESEM image (Fig. 2a), the resultant In_2O_3 sample was composed of numerous bundle-like crystals that were assembled with 1D nanorods. And the detailed morphology information of such microstructures was shown in Fig. 2(b and c). From the top-view SEM image (Fig. 2b), it can be observed that many 1D nanorods in the same plane vertically aligned around a single center, which was also constructed by numerous In_2O_3 rod-like crystals. Fig. 2c shows a side-view SEM image of the bundle-like microstructures. It was interesting to note that the growth direction of In_2O_3 nanorods were either parallel or perpendicular to a central symmetrical axial direction (indicated in the inset of Fig. 2c), leading to the formation of coaxial In_2O_3 nanorod bundles. In addition, the high-magnification SEM image was shown in Fig. 2d, as can be seen, the average diameter of In_2O_3 nanorods was about 50 nm and the nanorods were consisted of a large number of agglomerate nanoparticles.

Fig. 3a presents a typical TEM image of as-obtained In_2O_3 sample, from which the bundle-like hierarchical structures got further confirmed. Fig. 3b gives the detailed structural information of an individual In_2O_3 nanorod, the dark/light contrast indicated that the nanorod was composed of numerous nanoparticles, and thus many stacking pores were formed. Furthermore, the corresponding selected-area electron diffraction (SAED) pattern indicated that

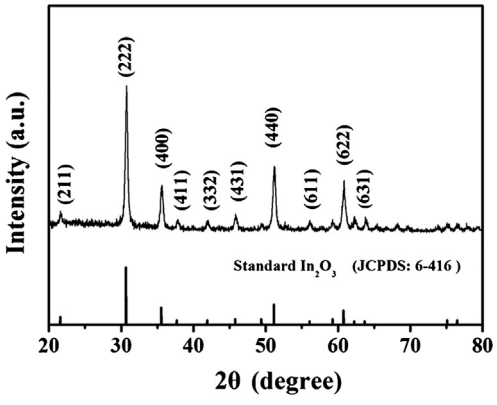

Fig. 1. X-ray diffraction pattern of the as-prepared In_2O_3 nanorod bundles.

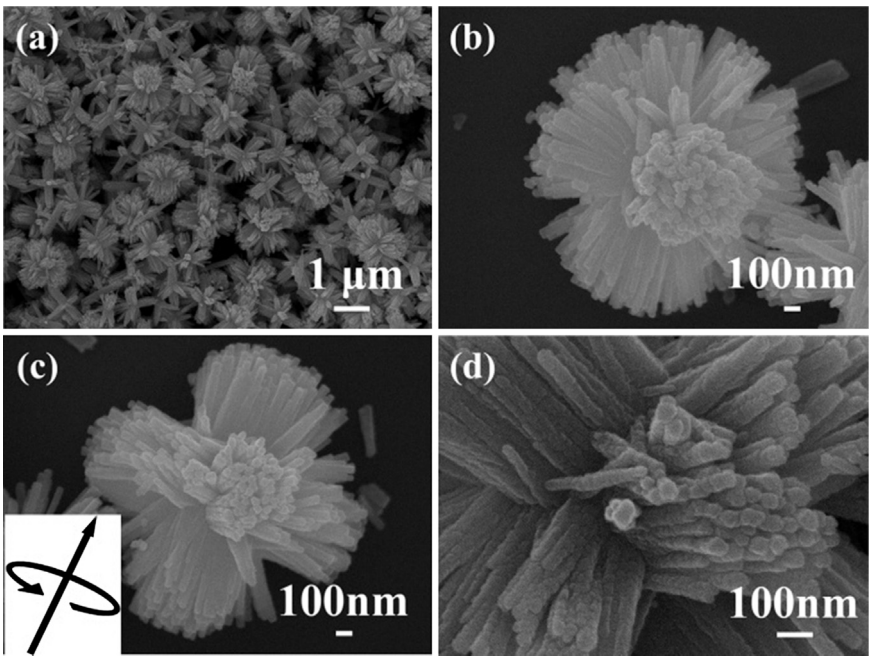

Fig. 2. SEM images of bundle-like In_2O_3: (a) low-magnification; (b) and (c) enlarged; (d) high-magnification.

the In_2O_3 nanorods were polycrystalline in nature, as shown in the inset of Fig. 3b. The HRTEM images taken from the rectangular regions of In_2O_3 nanorod were recorded in Fig. 3(c and d). It can be clearly seen that the In_2O_3 nanoparticles attached on the nanorods were highly crystallized and the lattice fringe spacing was about 0.292 nm, which was in good accordance with the distance between the {222} planes of cubic indium oxide.

It is well known that the porous structure plays an important role in facilitating the gas diffusion and improving the sensing properties of gas sensor. The nitrogen adsorption and desorption measurement was conducted to investigate the porous characteristic of the obtained In_2O_3 nanostructures. Fig. 4 shows nitrogen adsorption–desorption isotherm and corresponding pore size distribution plot of the as-obtained In_2O_3 sample. As can be seen, the adsorption–desorption isotherm exhibited an obvious hysteresis loop and could be indexed as type-IV isotherm according to the IUPAC classification, which confirmed the existence of mesoporous structures (2–50 nm) in the product. Pore diameter distribution (inset of Fig. 4) indicated that the pore size was mainly distributed around the average size of 13.5 nm. Furthermore, the BET surface area of the product was calculated to be 40.4 m^2/g based on the nitrogen adsorption isotherm.

In virtue of the precise control over heating procedure, microwave hydrothermal method made it possible to analyze the intermediates during the temperature-rise stage. Hence, to get a better understanding on the evolution processes of these bundle-like microstructures, a time-resolved observation had been characterized by scanning electron microscopy (SEM), as shown in

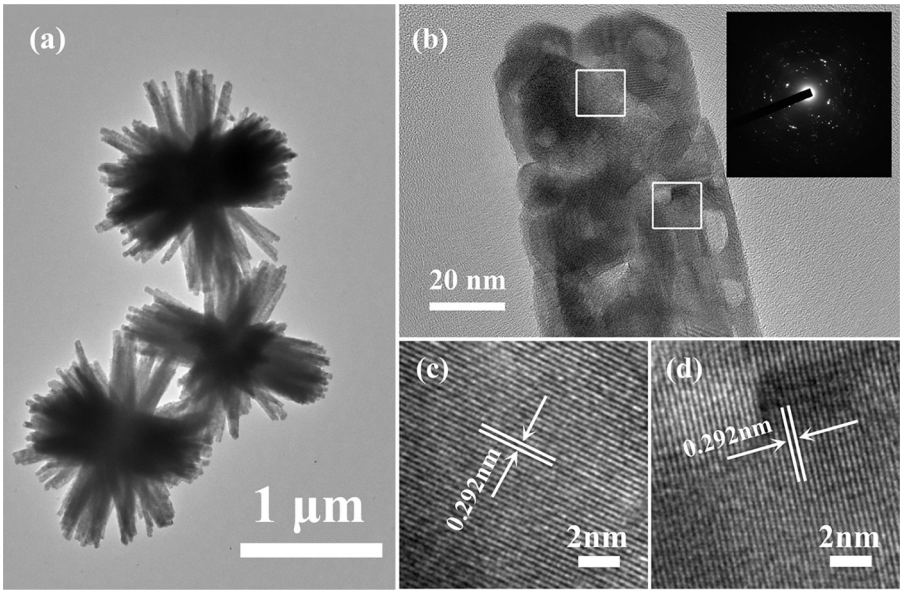

Fig. 3. (a) Typical TEM image of bundle-like In_2O_3; (b) TEM image and SAED pattern (inset) of a single nanorod; (c) and (d) HRTEM image taken from the area marked by rectangle.

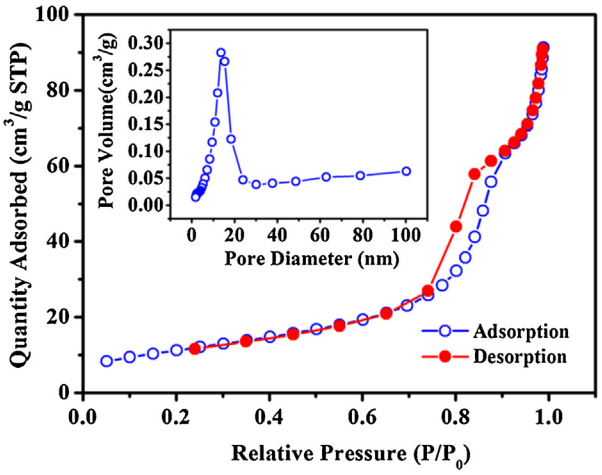

Fig. 4. Typical N_2 adsorption–desorption isotherm and the corresponding pore size distribution curve (inset) of In_2O_3 nanorod bundles.

Fig. 5(a–d). The SEM images of the sample collected from 115 °C (no precipitate generated below 115 °C) were shown in Fig. 5a and the inset. It can be seen that uniform elliptic nanoparticles with smooth surface had been formed, and the length of the obtained ellipsoid along long and short axis directions were about 850 nm and 800 nm, respectively. As the temperature increased to 120 °C, some small protuberances showed up on the surface of the above elliptic nanoparticles. Interestingly, these protuberances seem to prefer appearing at the position with bigger curvature (Fig. 5b and the inset). At 130 °C, accompany with the growth of the crystal, the protuberances on the surface gradually evolved into many 1D nanorods (Fig. 5c and the inset). When the hydrothermal procedure came to 140 °C, coaxial nanorod bundles were finally obtained, which could be seen from Fig. 5d and its inset. Even though detailed mechanism still needs more investigation, a plausible mechanism was proposed to explain the formation of In_2O_3 nanorods on the basis of the foregoing results. As demonstrated by Cho et al. and Shang et al. [35,36], vitamin C anions could adsorb onto the crystal surface because of their polar groups (–COO– and –OH), which will further hamper the crystal surface from directly contacting ambient solution and slow down the growth of crystal in all directions. Hence, the uniform nanoparticles were obtained at the beginning stage. Subsequently, along with the growth of initial crystal, the surface area increased simultaneously. Therefore, the molecules of vitamin C was not enough to cover every crystal surface anymore, which resulted in desorption of vitamin C from the surface (especially in the position with bigger curvature). As a result, the bare grains on the initial crystal got more chance to contact the ambient solution and eventually grew into many nanorods.

3.2. Gas sensing properties

Nitrogen dioxide (NO_2), known as one of notorious pollutants in air, has been threatening the environment by creating acid rain and photochemical smog. Thus, the development of gas sensors for monitoring the concentration of nitrogen dioxide has received growing attention because of its environmental importance [37]. Taking advantage of the as-obtained bundle-like In_2O_3 as sensing material, gas sensors used for detecting NO_2 were fabricated and their corresponding sensing performance were investigated in this study. Considering that the sensing behaviour of gas sensors based on most metal oxides depend closely on their operating temperature [38,39], the temperature dependent properties of the as-fabricated gas sensors were measured first. Fig. 6 shows the response of the sensor to 1 ppm NO_2 at different temperatures ranging from 50 to 175 °C. The results indicated that the response of sensor based on bundle-like In_2O_3 exhibited a typical "volcano" shape. It is well known that the response of sensors is related to the chemical reactions between the adsorbed oxygen species and the tested gas on the surface of oxides. At low temperatures the tested gas molecules do not have enough thermal energy to react with the surface adsorbed oxygen species. As the temperature increases, the gas molecules become activated enough to react with the surface adsorbed oxygen species. Therefore, the response kept increasing along with the operating temperature at first. However, if the temperature is too high, the gas adsorption is not adequately compensated by the increased chemical reaction, the response of the sensor begins to reduce upon further increasing the temperature

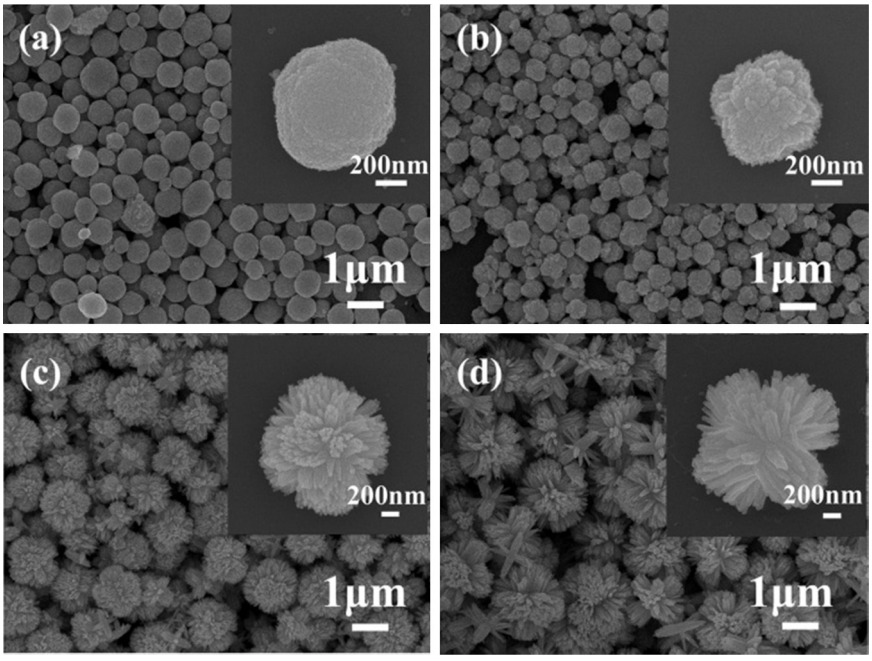

Fig. 5. Morphological characterization of In_2O_3 samples prepared with assistance of vitamin C at different reaction stage: (a) 115 °C; (b) 120 °C; (c) 130 °C; and (d) 140 °C.

Table 1
Comparison of gas-sensing performances of In_2O_3 gas sensors using different sensing materials.

Morphology of In_2O_3	Synthesis approach	NO_2 concentration	Operating temperature (°C)	Response (R_g/R_a)	Reference
Microspheres	Solvent-thermal	20 ppm	250	~37	[41]
Nanowires	Hydrothermal	1 ppm	250	2.57	[42]
Nanoplates	Hydrothermal	1 ppm	150	73	[43]
Thin films	Thermal oxidation	5 ppm	180	~10	[44]
Nanocrystals	Water bath	1 ppm	83	52.1	[45]
Bundle-like	Microwave hydrothermal	1 ppm	100	87	This work

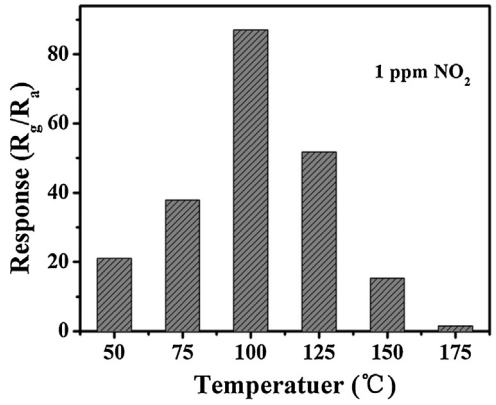

Fig. 6. Responses of the sensor as a function of operating temperature to 1 ppm NO_2.

[40]. In this case, the temperature of 100 °C was chosen as the optimum operating temperature of the gas sensors for detecting NO_2 gas, because the response to 1 ppm NO_2 reached a maximum value of 87 at this temperature. Besides, a comparison between the sensing performances of present sensor and some previous works is summarized in Table 1. It can be observed that the sensor based on unique bundle-like In_2O_3 exhibted an enhanced response than those in other literatures [41–45].

Fig. 7 presents the dynamic responses of the gas sensor when orderly exposed different concentrations of NO_2 at 100 °C. It is clear that the responses of the sensor increased rapidly with the concentration of NO_2 ranging from 150 to 1000 ppb. The gas responses to 150, 200, 300, 500, 700 and 1000 ppb NO_2 were about 9.8, 12.2, 20.8, 39, 56.7 and 87, respectively. Moreover, in order to clarify the low detection limit of the sensor, consecutive tests towards low-concentration NO_2 (below 100 ppb) were carried out. It is noteworthy that the sensor based on the bundle-like In_2O_3 still had an obvious response, even when the concentration of NO_2 was as low as 40 ppb (inset of Fig. 7).

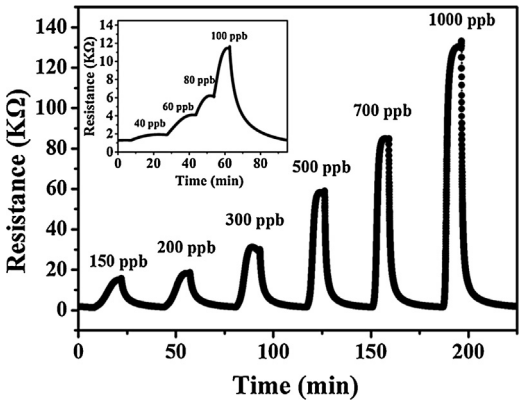

Fig. 7. Responses of the sensor upon exposure to different concentrations of NO_2 at optimal operation temperature.

To get further insight into sensing performance of the as-obtained gas sensor, the response and recover transients towards 1 ppm NO_2 were also measured at the optimum operating temperature. As can be seen from Fig. 8a, once the sensor contacted with NO_2, the resistance increased immediately and gradually reached a steady state. The corresponding response time for this process was about 177 s. Subsequently, the sensor was transferred into air to recover and the time taken during recovery was about 152 s. Fig. 8b shows several cycles of repeated test toward NO_2 gas. As can be seen, there was no obvious response attenuation when the sensor was alternately exposed to air and 1 ppm NO_2 gas, which demonstrated that the sensor based on bundle-like In_2O_3 had an excellent reversibility.

Fig. 9a displays the responses of the sensor towards various common interfering gases, such as Cl_2, O_3, H_2S, NH_3, SO_2, and C_2H_5OH. It can be clearly observed that the response of sensor based on bundle-like In_2O_3 towards NO_2 was remarkable higher than that towards other tested gases at operating temperature from 50 to 150 °C. For 1 ppm NO_2, the corresponding response was as high as 87 at 100 °C, while the responses to other gases were no greater than 10, even some of them had much higher concentration. By contrast, the sensor displayed a good selectivity to NO_2 gas. During practical application of gas sensor, except for the excellent selectivity, the stability is also very important. Therefore, the long-time stability of the gas sensor based on In_2O_3 nanorod bundles towards 1 ppm NO_2 was measured at 100 °C. As can be seen from Fig. 9b, the gas response of the sensor changed over time but nearly fluctuated around the initial value. This result indicates that such In_2O_3 nanorod bundles might be a good candidate for practical detection of NO_2 gas.

It is well known that gas sensing is a surface-related phenomenon, which involves the adsorption or desorption of gaseous molecules and the interaction (electronic or chemical) among these different kinds of gas molecules on the surface of sensing film [46,47]. When the In_2O_3 sensors were exposed to air atmosphere, the grains of In_2O_3 were naturally surrounded by ambient oxygen molecules, which could extract free electrons from the conduction of In_2O_3 causing the formation of chemisorbed oxygen species (O^{2-}, O^- or O_2^-) on the surface [48,49]. As a consequence, due to the reduction of electron concentration in the sensing material, a depletion layer was formed on the surface domains of In_2O_3. If target gas (NO_2) was introduced at this moment, due to its strong oxidizing characteristics [50], NO_2 molecules would harvest electrons either by directly extraction like oxygen molecules, or by the redox reactions with the adsorbed oxygen species on the surface of In_2O_3 (shown in Eq. (1) and (2)) [51,52]. Consequently, the thickness of depletion layer and the resistance of the sensor were increased.

$$NO_{2(gas)} + e^- \rightarrow NO_{2(ads)}^- \quad (1)$$

$$NO_{2(gas)} + 2O_{(ads)}^- \rightarrow NO_{2(ads)}^- + O_{2(gas)} + e^- \quad (2)$$

According to the previous reports, the performance of gas sensor is governed by many characters of sensing materials. Among them, the most critical factors are the category and utilization rate of the sensing material. Therefore, the rational choice and design

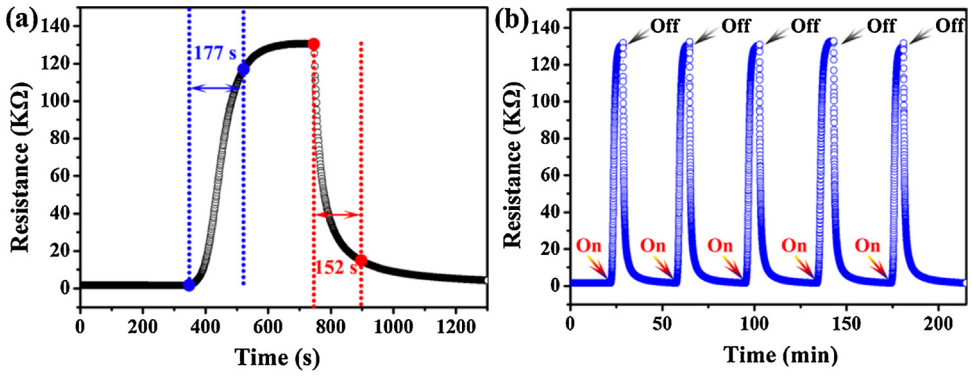

Fig. 8. (a) Transient response and recovery characteristic; (b) reproducibility of the sensor based on In_2O_3 nanorod bundles to 1 ppm NO_2 at 100 °C.

of sensing materials is very important for a successful gas sensor. In this study, the good performance of bundle-like In_2O_3 may be attributed to its excellent electric conductivity and its special structural advantage. As stated above, the response towards NO_2 was calculated according to the formula ($S = R_g/R_a$), low baseline resistance will be conducive to achieve high response. For the gas sensor based on as-obtained In_2O_3, the resistance in the air was only few Kohms. This means that during the subsequent detection of NO_2, a tiny enhancement in resistance would cause an obvious response. More importantly, the well-defined hierarchical configuration endowed the bundle-like In_2O_3 a high surface area and abundant porous structures, which would facilitate the gas diffusion toward the entire sensing materials [23]. Thus, the utilization rate of the sensing body was increased and a high sensitivity was finally observed.

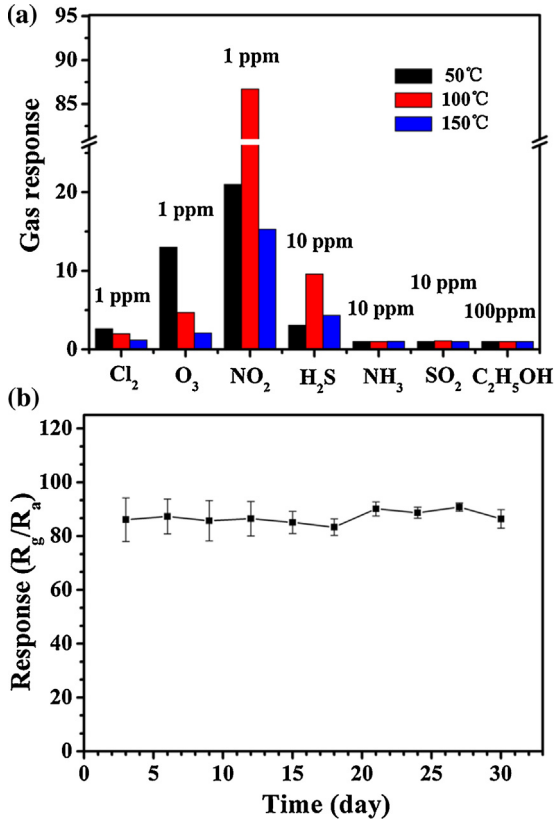

Fig. 9. (a) Responses of the sensor based on In_2O_3 nanorod bundles to various interfering gases at different temperature; (b) long-time stability of In_2O_3 nanorod bundles to 1 ppm NO_2 at 100 °C.

4. Conclusion

In summary, we have demonstrated the rapid synthesis of In_2O_3 nanorod bundles using biomolecules (vitamin C) as structure-directing agent via a microwave hydrothermal method. Remarkably, the observations of morphology evolution revealed that the well-aligned bundle-like In_2O_3 had been sucessfully built during the temperature-rise stage, which only demands 30 min. When evaluated as gas sensors, these In_2O_3 nanorod bundles exhibited a high response and good selectivity towards NO_2. At the optimum operating temperature, the response to 1 ppm NO_2 was as high as 87. The good sensing properties observed here were attributed to their hierarchical microstructures, which endowed the In_2O_3 nanorod bundles a high surface area and abundant porous structures.

Acknowledgements

This work is supported by the National Nature Science Foundation of China (Nos. 61374218, 61134010, 61304242, and 61327804), Program for Chang Jiang Scholars and Innovative Research Team in University (No. IRT13018) and National High-Tech Research and Development Program of China (863 Program, No. 2013AA030902 and 2014AA06A505).

References

[1] M.R. Alenezi, S.J. Henley, N.G. Emerson, S.R.P. Silva, From 1D and 2D ZnO nanostructures to 3D hierarchical structures with enhanced gas sensing properties, Nanoscale 6 (2014) 235–247.
[2] Y.F. Sun, S.B. Liu, F.L. Meng, J.Y. Liu, Z. Jin, L.T. Kong, J.H. Liu, Metal oxide nanostructures and their gas sensing properties: a review, Sensors 12 (2012) 2610–2631.
[3] J. Li, Y. Lu, Q. Ye, M. Cinke, J. Han, M. Meyyappan, Carbon nanotube sensors for gas and organic vapor detection, Nano Letters 3 (2003) 929–933.
[4] S.A. Waghuley, S.M. Yenorkar, S.S. Yawale, S.P. Yawale, Application of chemically synthesized conducting polymer-polypyrrole as a carbon dioxide gas sensor, Sens. Actuators B: Chem. 128 (2008) 366–373.
[5] X. Liu, S. Cheng, H. Liu, S. Hu, D. Zhang, H. Ning, A survey on gas sensing technology, Sensors 12 (2012) 9635–9665.
[6] A.A. Tomchenko, G.P. Harmer, B.T. Marquis, J.W. Allen, Semiconducting metal oxide sensor array for the selective detection of combustion gases, Sens. Actuators B: Chem. 93 (2003) 126–134.
[7] E. Comini, G. Faglia, G. Sberveglieri, Z. Pan, Z.L. Wang, Stable and highly sensitive gas sensors based on semiconducting oxide nanobelts, Appl. Phys. Lett. 81 (2002) 1869–1871.
[8] P. Li, H. Fan, Y. Cai, In_2O_3/SnO_2 heterojunction microstructures: facile room temperature solid-state synthesis and enhanced Cl_2 sensing performance, Sens. Actuators B: Chem. 185 (2013) 110–116.
[9] I. Hamberg, C. Granqvist, K. Berggren, B. Sernelius, L. Engström, Band-gap widening in heavily Sn-doped In_2O_3, Phys. Rev. B 30 (1984) 3240–3249.
[10] N. Du, H. Zhang, B.D. Chen, X.Y. Ma, Z.H. Liu, J.B. Wu, D.R. Yang, Porous indium oxide nanotubes: layer-by-layer assembly on carbon-nanotube templates and application for room-temperature NH_3 gas sensors, Adv. Mater. 19 (2007) 1641–1645.

[11] K.I. Choi, H.R. Kim, J.H. Lee, Enhanced CO sensing characteristics of hierarchical and hollow In_2O_3 microspheres, Sens. Actuators B: Chem. 138 (2009) 497–503.
[12] X. Li, J. Liu, H. Guo, X. Zhou, C. Wang, P. Sun, X. Hu, G. Lu, Au@In_2O_3 core–shell composites: a metal–semiconductor heterostructure for gas sensing applications, RSC Adv. 5 (2014) 545–551.
[13] J. Xu, X. Wang, J. Shen, Hydrothermal synthesis of In_2O_3 for detecting H_2S in air, Sens. Actuators B: Chem. 115 (2006) 642–646.
[14] M. Ali, C.Y. Wang, C.C. Roehlig, V. Cimalla, T. Stauden, O. Ambacher, NO_x sensing properties of In_2O_3 thin films grown by MOCVD, Sens. Actuators B: Chem. 129 (2008) 467–472.
[15] J. Zhao, T. Yang, Y. Liu, Z. Wang, X. Li, Y. Sun, Y. Du, Y. Li, G. Lu, Enhancement of NO_2 gas sensing response based on ordered mesoporous Fe-doped In_2O_3, Sens. Actuators B: Chem. 191 (2014) 806–812.
[16] P. Li, H. Fan, Y. Cai, M. Xu, C. Long, M. Li, S. Lei, X. Zou, Phase transformation (cubic to rhombohedral): the effect on the NO_2 sensing performance of Zn-doped flower-like In_2O_3 structures, RSC Adv. 4 (2014) 15161–15170.
[17] P. Li, H. Fan, Y. Cai, M. Xu, Zn-doped In_2O_3 hollow spheres: mild solution reaction synthesis and enhanced Cl_2 sensing performance, CrystEngComm 16 (2014) 2715–2722.
[18] P. Li, Y. Cai, H. Fan, Porous thin sheet-based α-Fe_2O_3-doped In_2O_3 structures: hydrothermal synthesis and enhanced Cl_2 sensing performance, RSC Adv. 3 (2013) 22239–22245.
[19] F. Caruso, Nanoengineering of particle surfaces, Adv. Mater. 13 (2011) 11–22.
[20] P. Sun, Y. Liu, X. Li, Y. Sun, X. Liang, F. Liu, G. Lu, Facile synthesis and gas-sensing properties of monodisperse α-Fe_2O_3 discoid crystals, RSC Adv. 2 (2012) 9824–9829.
[21] Y. Chen, C. Zhu, T. Wang, The enhanced ethanol sensing properties of multi-walled carbon nanotubes/SnO_2 core/shell nanostructures, Nanotechnology 17 (2006) 3012–3017.
[22] X. Zhou, W. Feng, C. Wang, X. Hu, X. Li, P. Sun, K. Shimanoe, N. Yamazoe, G. Lu, Porous ZnO/$ZnCo_2O_4$ hollow spheres: synthesis, characterization, and applications in gas sensing, J. Mater. Chem. A (2014) 17683–17690.
[23] J.-H. Lee, Gas sensors using hierarchical and hollow oxide nanostructures: overview, Sens. Actuators B: Chem. 140 (2009) 319–336.
[24] G. Li, C. Liu, Y. Liu, Facile fabrication of hollow mono-dispersed TiO_2 spheres in an aqueous solution, J. Am. Ceram. Soc. 90 (2007) 2667–2669.
[25] Z.-X. Yang, W. Zhong, Y. Deng, C.-T. Au, Y.-W. Du, Design and synthesis of novel single-crystalline hierarchical CdS nanostructures generated by thermal evaporation processes, Cryst. Growth Des. 11 (2011) 2172–2176.
[26] J.Y. Lao, J.G. Wen, Z.F. Ren, Hierarchical ZnO nanostructures, Nano Letters 2 (2002) 1287–1291.
[27] D.I. Suh, S.Y. Lee, T.H. Kim, J.M. Chun, E.K. Suh, O.B. Yang, S.K. Lee, The fabrication and characterization of dye-sensitized solar cells with a branched structure of ZnO nanowires, Chem. Phys. Lett. 442 (2007) 348–353.
[28] S.H. Ko, D. Lee, H.W. Kang, K.H. Nam, J.Y. Yeo, S.J. Hong, C.P. Grigoropoulos, H.J. Sung, Nanoforest of hydrothermally grown hierarchical ZnO nanowires for a high efficiency dye-sensitized solar cell, Nano Letters 11 (2011) 666–671.
[29] M. Mo, J.C. Yu, L. Zhang, S.K. Li, Self-assembly of ZnO nanorods and nanosheets into hollow microhemispheres and microspheres, Adv. Mater. 17 (2005) 756–760.
[30] C. Cheng, B. Liu, H. Yang, W. Zhou, L. Sun, R. Chen, S.F. Yu, J. Zhang, H. Gong, H. Sun, H.J. Fan, Hierarchical assembly of ZnO nanostructures on SnO_2 backbone nanowires: low-temperature hydrothermal preparation and optical properties, ACS Nano 3 (2009) 3069–3076.
[31] M. Baghbanzadeh, L. Carbone, P.D. Cozzoli, C.O. Kappe, Microwave-assisted synthesis of colloidal inorganic nanocrystals, Angew. Chem. Int. Ed. 50 (2011) 11312–11359.
[32] I. Bilecka, M. Niederberger, Microwave chemistry for inorganic nanomaterials synthesis, Nanoscale 2 (2010) 1358–1374.
[33] X. Li, W. Feng, Y. Xiao, P. Sun, X. Hu, K. Shimanoe, G. Lu, N. Yamazoe, Hollow zinc oxide microspheres functionalized by Au nanoparticles for gas sensors, RSC Adv. 4 (2014) 28005–28010.
[34] X. Li, X. Zhou, H. Guo, C. Wang, J. Liu, P. Sun, F. Liu, G. Lu, Design of Au@ZnO yolk-shell nanospheres with enhanced gas sensing properties, ACS Appl. Mater. Interfaces 6 (2014) 18661–18667.
[35] T.-M. Shang, J.-H. Sun, Q.-F. Zhou, M.-Y. Guan, Controlled synthesis of various morphologies of nanostructured zinc oxide: flower, nanoplate, and urchin, Cryst. Res. Technol. 42 (2007) 1002–1006.
[36] S. Cho, H. Jeong, D.H. Park, S.H. Jung, H.J. Kim, K.H. Lee, The effects of vitamin C on ZnO crystal formation, Crystengcomm 12 (2010) 968–976.
[37] H.-C. Cho, S. Takase, J.-H. Song, Y. Shimizu, Sensing behavior of solid-state impedancemetric NO_x sensor using solid electrolyte transducer and oxide receptor, Sens. Actuators B: Chem. 187 (2013) 94–98.
[38] A.K. Batra, A.K. Chilvery, P. Guggilla, M. Aggarwal, J.R. Currie, Micro- and nano-structured metal oxides based chemical sensors: an overview, J. Nanosci. Nanotechnol. 14 (2014) 2065–2085.
[39] Y. Chen, C.L. Zhu, G. Xiao, Reduced-temperature ethanol sensing characteristics of flower-like ZnO nanorods synthesized by a sonochemical method, Nanotechnology 17 (2006) 4537–4541.
[40] G. Neri, A. Bonavita, G. Micali, G. Rizzo, E. Callone, G. Carturan, Resistive CO gas sensors based on In_2O_3 and $InSnO_x$ nanopowders synthesized via starch-aided sol–gel process for automotive applications, Sens. Actuators B: Chem. 132 (2008) 224–233.
[41] Z. Cheng, L. Song, X. Ren, Q. Zheng, J. Xu, Novel lotus root slice-like self-assembled In_2O_3 microspheres: synthesis and NO_2-sensing properties, Sens. Actuators B: Chem. 176 (2013) 258–263.
[42] P. Xu, Z. Cheng, Q. Pan, J. Xu, Q. Xiang, W. Yu, Y. Chu, High aspect ratio In_2O_3 nanowires: synthesis, mechanism and NO_2 gas-sensing properties, Sens. Actuators B: Chem. 130 (2008) 802–808.
[43] X. Xu, X. Li, W. Wang, B. Wang, P. Sun, Y. Sun, G. Lu, In_2O_3 nanoplates: preparation, characterization and gas sensing properties, RSC Adv. 4 (2014) 4831–4835.
[44] T. Siciliano, M. Di Giulio, M. Tepore, A. Genga, G. Micocci, A. Tepore, In_2O_3 films prepared by thermal oxidation of amorphous InSe thin films, Thin Solid Films 520 (2012) 2455–2460.
[45] C. Chen, Y. Wei, D. Chen, X. Jiao, Indium oxide nanocrystals: capping-agent-free synthesis, size-control mechanism, and high gas-sensing performance, Mater. Chem. Phys. 125 (2011) 299–304.
[46] N. Yamazoe, K. Shimanoe, Theoretical approach to the rate of response of semiconductor gas sensor, Sens. Actuators B: Chem. 150 (2010) 132–140.
[47] M. Yuasa, T. Kida, K. Shimanoe, Preparation of a stable sol suspension of Pd-loaded SnO_2 nanocrystals by a photochemical deposition method for highly sensitive semiconductor gas sensors, ACS Appl. Mater Interfaces 4 (2012) 4231–4236.
[48] N. Yamazoe, G. Sakai, K. Shimanoe, Oxide semiconductor gas sensors, Catal. Surveys Asia 7 (2003) 63–75.
[49] A. Heilig, N. Bârsan, U. Weimar, M. Schweizer-Berberich, J.W. Gardner, W. Göpel, Gas identification by modulating temperatures of SnO_2-based thick film sensors, Sens. Actuators B: Chem. 43 (1997) 45–51.
[50] J.H. Jun, J. Yun, K. Cho, I.-S. Hwang, J.-H. Lee, S. Kim, Necked ZnO nanoparticle-based NO_2 sensors with high and fast response, Sens. Actuators B: Chem. 140 (2009) 412–417.
[51] Z. Dai, C.-S. Lee, Y. Tian, I.-D. Kim, J.-H. Lee, Highly reversible switching from P- to N-type NO_2 sensing in a monolayer Fe_2O_3 inverse opal film and the associated P–N transition phase diagram, J. Mater. Chem. A 3 (2015) 3372–3381.
[52] A. Afzal, N. Cioffi, L. Sabbatini, L. Torsi, NO_x sensors based on semiconducting metal oxide nanostructures: progress and perspectives, Sens. Actuators B: Chem. 172 (2012) 25–42.

Biographies

Xiaowei Li received his master's degree from Electronics Science and Engineering Department, Jilin University, China in 2013. That same year, he entered the PhD course and majored in microelectronics and solid state electronics. Presently, he is engaged in the microwave assisted synthesis and characterization of the semiconducting functional materials applied in gas sensors.

Shiting Yao is graduated from Changchun University of Science and Technology at the Science College in 2014. The same year, she joined Jilin University as a graduate and majored in the Integrated Circuit Engineering.

Jiangyang Liu received her BS degree from Electronics Science and Engineering department, Jilin University, China in 2014. Presently, she is a graduate student and majored in microelectronics and solid state electronics.

Peng Sun received his MS degree from State Key Laboratory of Superhard Materials, Jilin University, China in 2009. He entered the PhD course in 2010, majored in microelectronics and solid state electronics. His research interests lies in the synthesis and characterization of the semiconducting functional materials and gas sensors.

Yanfeng Sun received his PhD degree from Jilin University of China in 2007. Now he is an associate professor of Electronics Science and Engineering Department in Jilin University. His current researches focus on the nanoscience and gas sensor.

Yuan Gao obtained her PhD degree from Jilin University, China in 2012. Presently, she is working as lecturer in Electronics Science and Engineering Department of Jilin University. Her current research interests are the fabrication of graphene and semiconductor nanomaterials.

Geyu Lu received his BS and MS degree in electronic sciences in 1985 and 1988 from Jilin University in China, respectively, and PhD degree in 1998 from Kyushu University in Japan. Now he is a professor of Jilin University, China. Presently, he is interested in the development of functional materials and chemical sensors.